The effect of particle size distributions on the microstructural evolution during sintering

Bjørk, Rasmus; Tikare, V.; Frandsen, Henrik Lund; Pryds, Nini

Published in:
American Ceramic Society. Journal

Link to article, DOI:
10.1111/jace.12100

Publication date:
2013

Published in Journal of the American Ceramic Society, Vol. 96 (1), 103-110, 2013
DOI: 10.1111/jace.12100

The effect of particle size distributions on the microstructural evolution during sintering

R. Bjørk[1], V. Tikare[2], H. L. Frandsen[1] and N. Pryds[1]

Abstract
Microstructural evolution and sintering behavior of powder compacts composed of spherical particles with different particle size distributions (PSDs) were simulated using a kinetic Monte Carlo model of solid state sintering. Compacts of monosized particles, normal PSDs with fixed mean particle radii and a range of standard deviations, and log-normal PSDs with fixed mode and a range of skewness values were studied. Densification rate and final relative density were found to be inversely proportional to initial PSD width. Grain growth was faster during the early stages of sintering for broad PSDs, but the final grain sizes were smaller. These behaviors are explained by the smallest grains in the broader PSDs being consumed very quickly by larger neighboring grains. The elimination of the small grains reduces both the total number of necks and the neck area between particles, which in turn reduces the regions where vacancies can be annihilated, leading to slower densification rates. The loss of neck area causes grain growth by surface diffusion to become the dominant microstructural evolution mechanism, leading to poor densification. Finally, pore size was shown to increase with the width of PSDs, which also contributes to the lower densification rates.

[1] *Department of Energy Conversion and Storage, Technical University of Denmark - DTU, Frederiksborgvej 399, DK-4000 Roskilde, Denmark*
[2] *Sandia National Laboratory, Albuquerque, NM 87185, New Mexico, USA*
*__Corresponding author__: rabj@dtu.dk

1. Introduction

Sintering is an important technological process used to manufacture almost all ceramics and many metals from compacted powder particles. The powder compacts densify with accompanying dimensional changes resulting in mechanical strengthening, possible gastight microstructures and improved conductivity. Technologies today demand that the final microstructure be within very tight tolerances of grain size, pore size, macro-dimensional shape changes and other properties. Many processing conditions and powder characteristics, such as sintering temperature, time, atmosphere, application of load, powder purity, additives, pore formers, particle size distribution and others, can be varied to meet the tolerance requirements. Among these, particle size distribution is one of the most important and easiest to control. In this work, we examine the effect of a particle size distribution (PSD) on sintering behavior by isolating it as the sole variable during sintering.

Much is known about the effects of PSDs on sintering. In the early years of sintering science, it was thought that broad PSDs with higher green relative densities would result in higher final relative densities with better mechanical properties. However, it has been shown experimentally, numerically and analytically that sintering powder compacts with narrow PSDs, despite their lower green relative densities result in more homogeneous microstructures with higher final relative densities. Sintering of powders with both normal and log-normal PSDs have been studied as powder preparation techniques can result in both distributions (1).

Experimental comparison of narrow and broad PSDs of both Al_2O_3 and single-crystal tungsten showed the broad PSDs densified at a higher rate during early stages of sintering (1; 2; 3). This was attributed to the higher particle packing and the higher average number of nearest neighbor contacts per particle. In contrast, the narrow PSDs sintered to a higher final relative densities. Similar results were obtained for log-normal PSDs both analytically (4) and experimentally (5). For the tungsten powder the narrow PSD was also observed to exhibit a more uniform sized and spaced pore structure. These results differed from those of previous investigations using spherical copper particles. The very narrow PSD in the earlier study did not sinter to a higher relative density than the slightly broader ones (6). It was speculated that the difference between the two findings could be the forced packing of the tungsten, which could lead to a relatively finer pore structure than for the copper particles. In another study of PSDs with varying geometric standard deviation it was shown that the powder with intermediate PSDs sintered to higher relative density (7). The authors in this study concluded that other sintering variables were dominating over the PSDs.

Similar results to the Al_2O_3 and tungsten studies were reported for sintering simulated by the discrete element method (DEM) of normal, log-normal or bimodal PSDs. In this study densification rate was found to decrease with increasing distribution width (8). The increase in coordination number for large particle size was concluded to cause the decrease in den-

sification rate. Analytical calculations on tetrakaidecahedron shaped grains have also showed that narrow PSDs sinter to a higher relative density and that the shrinkage rate decreases significantly with increased width of the distribution (9; 10).

While there is general consensus in the literature that narrow PSDs lead to denser, more uniform sintered products, only one study has systematically varied the width of the PSD, to study its effects on sintering behavior. Furthermore this study only considered log-normal PSDs with no detailed analysis of the microstructural evolution. The mechanism causing the poor sintering behavior of broad PSDs has not been properly explained on a microstructural level and still remains an open question.

The objective of this work is to study the effect of a PSD on sintering, so that a mechanistic understanding of the densification and microstructural evolution behavior can be gained. To this end, we simulate microstructural evolution during sintering of powder compacts as a function of monosized, normal and log-normal PSDs at a sufficiently large scale (hundreds to thousands of particles) so that the microstructure can be characterized in detail continuously throughout the sintering process. A kinetic Monte Carlo (kMC) model that incorporates all the materials processes necessary to simulate simple solid-state sintering is used (11). Unlike DEM, grain growth, and grain and pore shape changes can be studied with this model (8) and at a larger scale with more particles of different sizes than possible using a surface evolver approach (12). Using numerical simulations allow all other sintering process variables such as grain shape, agglomeration and packing defects to be kept constant.

2. The numerical model

The sintering model used is a three dimensional statistical-mechanical kMC model. The microstructure is represented as an ensemble of material particles (not to be confused with powder particles) populating a cubic grid such that each ensemble particle occupies a voxel site. Microstructural features such as grains, pores, grain boundaries and pore surfaces are resolved. The model is able to incorporate all the processes necessary to simulate simple solid-state sintering. These are curvature-driven grain growth with the drag force of pinning but mobile pores, pore migration by surface diffusion, vacancy formation at pore surfaces with vacancy concentration given by the Gibbs-Thomson relation, grain boundary diffusion of the vacancies and finally vacancy annihilation at grain boundaries. Only a brief description of the model is given here as it has been described in detail in previous works (11; 13). The evolution during sintering is driven by minimization of the total interfacial free energy, quantified by the number of unlike neighbors a given voxel site has.

The system is evolved by ”moves“ that manipulate the ensemble of particles to simulate materials processes. Two randomly chosen neighboring sites are exchanged to simulate surface and grain boundary diffusion, and vacancy generation. Grain growth is simulated by changing membership of grain boundary grain sites from one grain to another. Annihilation is simulated by collapsing a column of sites from an isolated pore site at a grain boundary to the surface of the sample to simulate densification. If a move lowers the total energy of the system then the move is accepted. If the energy is increased the move is accepted with a probability calculated using the standard Metropolis algorithm. The model parameters can be adjusted to obtain the desired interfacial energies, namely grain boundary and pore surface energies. The diffusion rates can also be adjusted by attempting the different events with different frequencies. The simulation temperature for vacancy generation can also be adjusted to control the vacancy generation rate. By tuning these parameters, sintering conditions in the simulation can be matched to those of real materials. Free sintering with no constraining forces is simulated.

The units used in the kMC model warrant some attention. Time in the model is measured in Monte Carlo steps (MCSs). One MCS has passed when the number of attempted grain growth moves equals the total number of grain sites in the system. Time measured in MCS is linearly related to real time (11). The length scale of a cubic voxel is linearly proportional to real length. The linear relation between kMC time and real time will depend on the chosen length scale of the model. Energy is given in units of bond energy between unlike neighboring sites. The unlike neighbor bond at pore surfaces have the same energy as those at grain boundaries giving the condition that pore surface energy is the same as grain boundary energy in the simulations with a dihedral angle $\psi = 60^\circ$. While most materials have higher grain boundary energy, we have chosen them to be equal for simplicity and densification will occur for this condition. The scaling of MCS to time can be determined by comparing the modeled system with a similar experimental system. Using this approach the kMC model has previously been used to model the sintering of copper spheres as observed using X-ray tomography, where very good agreement between modeling and experiment results were seen (11). The model has also been used to study the sintering of close-packed spheres (15) where the model confirmed and expanded previously reported experimental results.

The simulation parameters used for this study are a temperature for grain growth and pore migration of $k_BT = 1$ and for vacancy formation of $k_BT = 15$. The attempt frequencies were chosen in the ratio 1:1:5 for grain growth, pore migration and vacancy formation, respectively. The values for the temperatures and attempt frequencies were chosen such that the modeled samples displayed a realistic sintering behavior for a powder compact.

2.1 Generating the powder compact

Powder compacts of spherical particles with radii that follow a normal or log-normal distributions are generated by simulating the pouring of spherical particles of the desired PSD into a cubic container $300 \times 300 \times 300$ voxels. The numerical code used to simulate pouring and packing is a modified version of

the Large-scale Atomic/Molecular Massively Parallel Simulator (LAMMPS) code, available as open source from Sandia National Laboratories. Each powder particle is a single crystal and it is thus equivalent to speak of grains and particles in this work.

One monosized, six normal and four log-normal PSDs were packed to form powder compacts. The normal PSDs are characterized by the mean, μ, and the standard deviation, σ. The mean particles radius is held constant at μ = 10 voxel lengths and the standard deviation is varied from σ = 0.5 to 3.0 in increments of 0.5. The log-normal PSDs are characterized by the mode and skewness. The mode is the most frequently occurring value in the distribution, and the skewness is a measure of the asymmetry of the distribution. These parameters are the natural parameters to vary for a log-normal distribution. The skewness, denoted γ, is defined as the third standardized moment, $\gamma = \mu_3/\sigma^3$, where μ_3 is the third moment about the mean. Given the mean, μ, and the standard deviation, σ, are those of the logarithm of the distribution, the mode of the log-normal distribution is given by $mode = e^{\mu-\sigma^2}$ and the skewness by $\gamma = \left(e^{\sigma^2}+2\right)\sqrt{(e^{\sigma^2}-1)}$. The mode of the log-normal distribution is fixed at the same value as the mean for the normal distribution, and the skewness is varied from γ = 0.25 to 1.0 in increments of 0.25. The initial cumulative distributions of the normal and log-normal distributions are shown in Fig. 1. The size is given as the equivalent radius, which is defined as $r_{\text{equi}} = (\frac{3}{4}\frac{1}{\pi}V)^{1/3}$, where V is the volume of a particle. Also shown on the figure are analytically calculated cumulative distribution functions for the corresponding normal and log-normal distributions. The generated distributions closely match the theoretically calculated distributions.

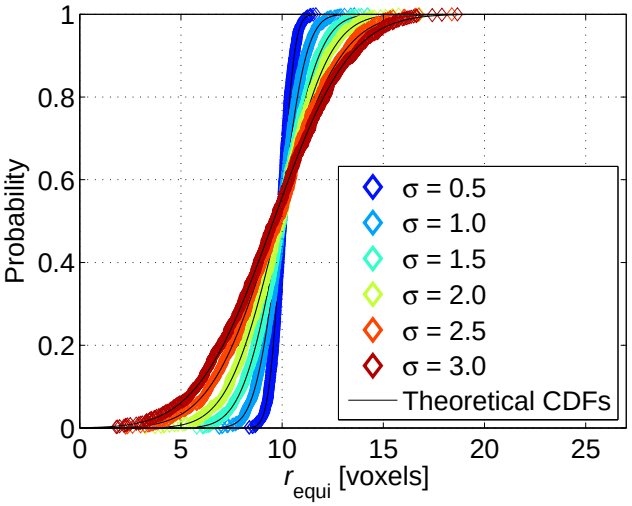

(a) Normal distributions

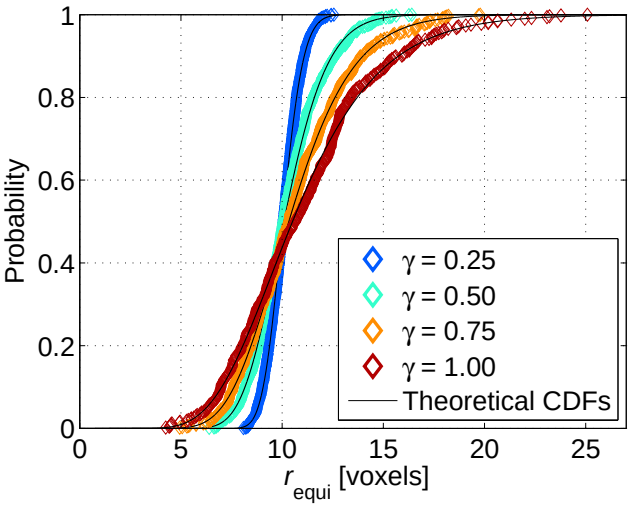

(b) Log-normal distributions

Figure 1. The initial cumulative distribution functions (CDF) for (a) the normal and (b) log-normal distributions of the particle sizes. Also shown are the theoretically calculated CDFs for the given distribution parameters.

3. Resulting sintering behavior and microstructural evolution

The isothermal sintering behavior of powder compacts composed of differing PSDs is investigated by characterization of the microstructure, relative density, grain size, pore size and connectivity, and grain coordination. The microstructure is analyzed periodically at increments of 16,000 MCS during the simulation. All simulations are run for the same length of time, which, as explained previously, scales linearly with physical time. Furthermore, the simulation time can be directly compared as the mode of the initial PSDs are all the same. While the sintering of the entire powder compact is simulated, only the microstructure in the central homogeneous part of the sample is analyzed to minimize edge effects introduced by the finite size of the sample. The density measured is always the relative density, ρ, which is defined as one minus the fraction of porosity. The average grain size is denoted $\overline{G}$ and is given in units of r_{equi}.

3.1 The microstructure of the sintered samples

Slices through the center of the microstructures of three powder compacts with different PSDs at the beginning and end of simulated sintering are shown in Figs. 2 and 3, respectively. The three distributions are monosized, normal with standard deviation σ= 2.0 and log-normal with skewness γ= 1.0. Initially the normal and log-normal PSDs can be seen to have a number of particles that are much larger than those seen in the monosized compact. At the end of sintering more pores are seen in the compacts with normal and log-normal PSDs.

3.2 Relative density and grain size evolution

The densification curves for the normal and log-normal PSDs are shown in Fig. 4. The broader the distribution the lower the

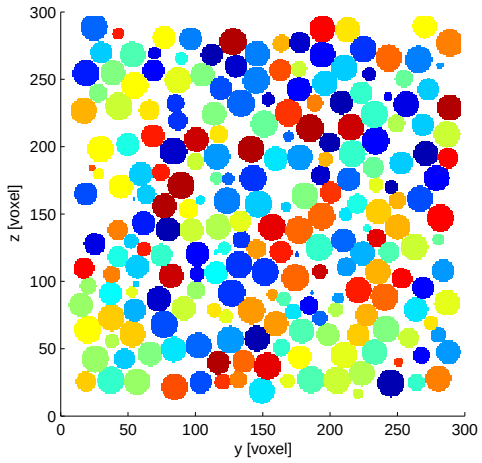

(a) Monosized distribution

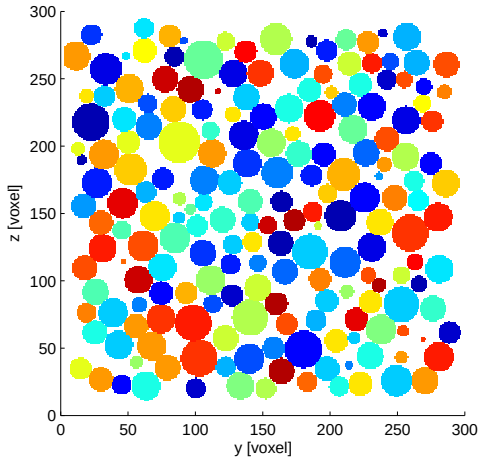

(b) Normal distribution

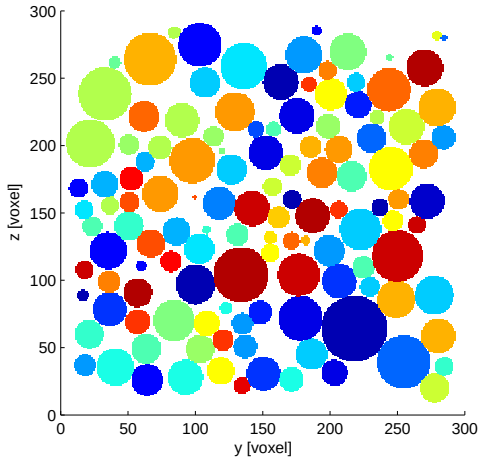

(c) Log-normal distribution

Figure 2. A slice through the center of the microstructure at the beginning of sintering for (a) the monosized, (b) the normal distribution with $\sigma = 2$ and (c) the log-normal distribution with $\gamma = 1.00$ samples. The coloring of the grains are so that these can be distinguished.

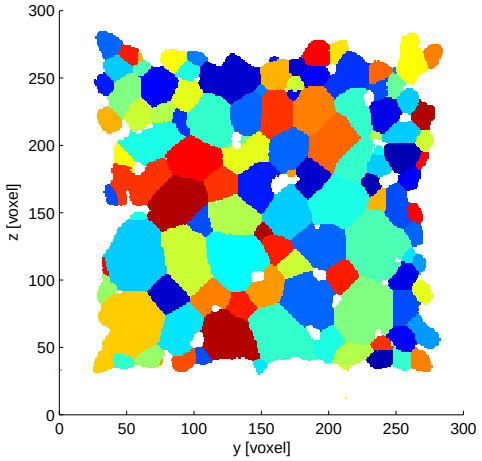

(a) Monosized distribution

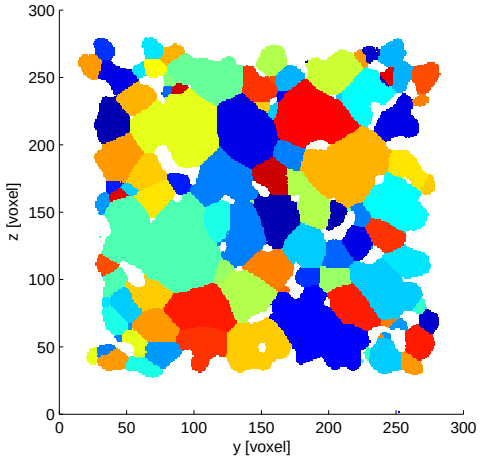

(b) Normal distribution

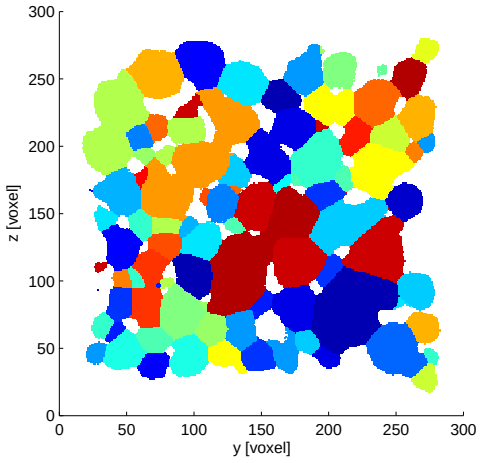

(c) Log-normal distribution

Figure 3. A slice through the center of the microstructure at the longest sintering time for (a) the monosized, (b) the normal distribution with $\sigma = 2$ and (c) the log-normal distribution with $\gamma = 1.00$ samples. The time corresponds to 192000 MCS. The coloring of the grains are so that these can be distinguished.

final density and the higher the initial grain growth rate is. It is well known that grain growth is limited in the initial stage of sintering and increase as sintering progresses(16). To examine the relationship between grain growth and densification, the average grain size is plotted as a function of relative density for all PSDs in Fig. 5. The starting mean grain size for the log-normal distributed powders increases with skewness, even though the mode is kept constant. Note that the initial relative density increases with the width of the PSDs. This is expected as the small particles in the broad PSDs fill the interstices between larger particles, leading to a higher initial relative density. During sintering the average grain size increases as a function of relative density for all PSDs, but the onset of growth is at higher densities for the narrower distributions. Furthermore, the rate of increase in grain size as a function of relative density is higher when the grow onset is at higher densities. As a consequence the grain size of monosized particles increases rapidly with relative density with the onset of growth at relative density well above $\rho = 0.90$.

These observations are supported by pore intercept length measurements on the initial powder compacts for the PSDs. Pore intercept length was measured along 1000 randomly-placed and randomly-oriented straight lines in three dimensional space throughout the central homogeneous portion of each powder compact. The results are shown in Fig. 6, which show pore intercept length as a function of standard deviation and skewness at the beginning of sintering. The average pore intercept length is longest for the samples with broadest PSDs, especially for the log-normal distributions. These samples also had the largest standard deviations of the intercept pore length. Since these samples contain larger pores, they will be more difficult to sinter to higher relative density without grain growth, exactly as seen in Fig. 5. Thus the pore structure in the powder compacts mirrors the experimental observation of Patterson & Griffin (1), i.e. that the narrow distributions have a more uniform pore structure than the broader distributions. However, the reason why the grain growth occurs early in the samples with broad size distributions is not only due to the pore size distribution, as this remains fairly constant for the normal PSDs. A possible explanation to this behavior is that the sintering behavior and microstructural evolution can be affected by the small grains in a given PSD. The pore intercept length during sintering is not shown, as it remains constant after an initial decline in the early stage of sintering. This is also observed for the sintering of alumina (17), and could be explained by pore collapse and breakup (18).

3.3 Distribution parameters during sintering

The influence of small grains on the sintering behavior and microstructural evolution has been carefully examined. Small grains were characterized as grains smaller than 90% of the initial mode of that PSD. In Fig. 7 the fraction of small grains as function of relative density for the different PSDs is shown. As can be seen, for the broad distributions the number of small grains decreases rapidly, showing that these

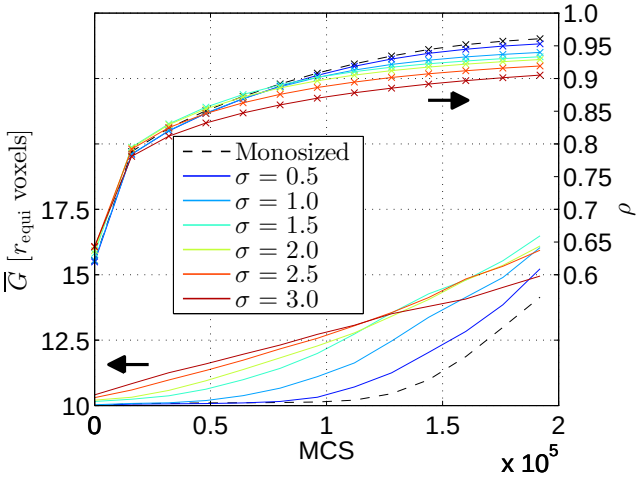

(a) Normal distributions

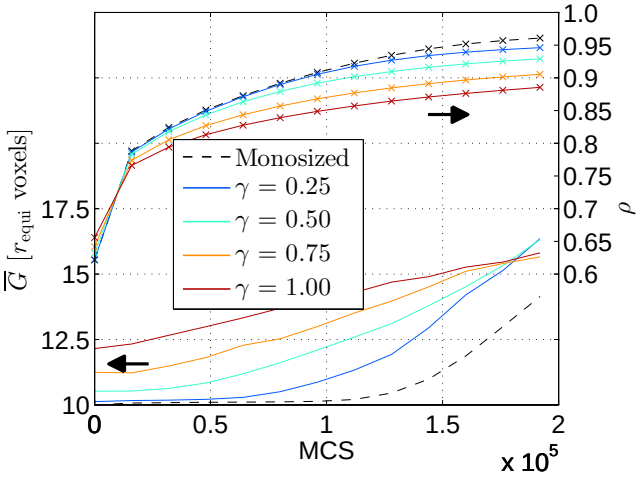

(b) Log-normal distributions

Figure 4. The evolution of relative density and grain size as a function of time, measured in MCS, for (a) the normal and (b) log-normal distributions.

are quickly consumed by larger neighboring grains. For the narrow distributions only a small number of grains are initially below 90% of the initial mode, but as sintering progresses and grains grow, some particles begins to shrink and the number of small grains increases. This happens until the small grains are consumed by the large grains, which again lowers the number of small grains. This explanation is supported by the data presented in Fig. 8 which shows normalized standard deviation of grain size, $\sigma/\overline{G}$, as function of relative density for the different PSDs. The broad PSDs show a relatively small change in $\sigma/\overline{G}$. As the small grains are consumed by theirs neighbors, the absolute grain sizes shifts to larger sizes and the distributions broadens slightly. However, for the narrow PSDs, the smaller grains become smaller, but still persist to higher densities, while the larger grains grow. This broadens the distribution increasing the relative standard deviation. Other

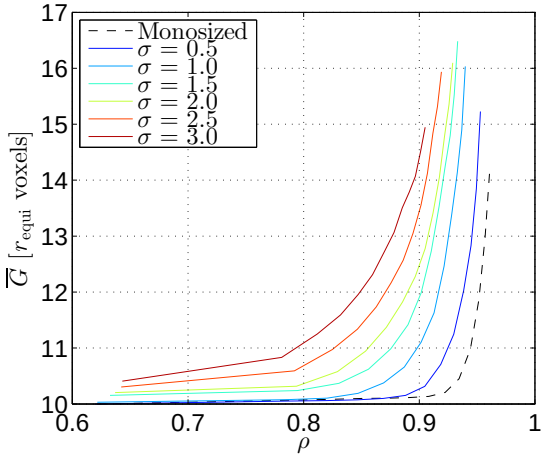

(a) Normal distributions

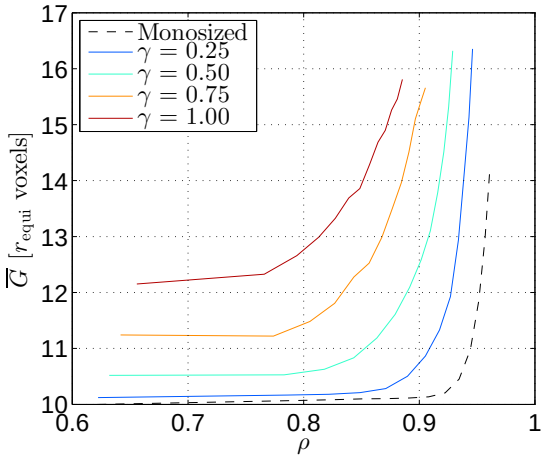

(b) Log-normal distributions

Figure 5. The evolution of grain size as a function of the relative density for (a) the normal and (b) log-normal distributions.

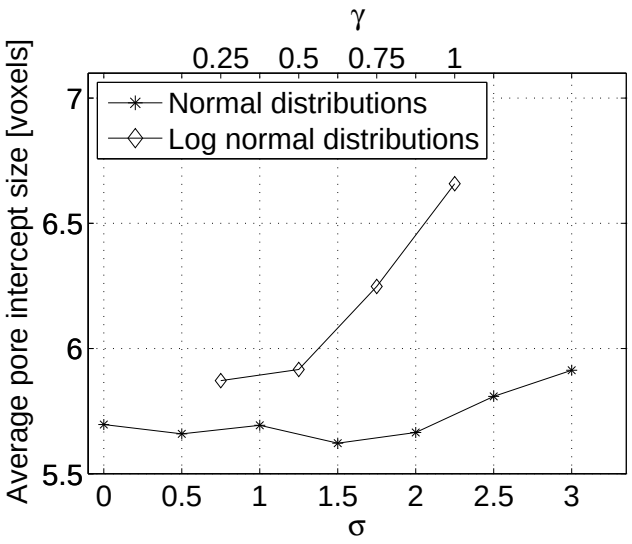

Figure 6. The average pore intercept size as function of the standard deviation, σ, or the skewness, γ, at the beginning of sintering. The distribution with $\sigma = 0$ is the monosized distribution.

definitions of small grains, e.g. 70% and 80% of the initial mode, has also been tried and the conclusion remains the same. The exact position of the peaks in Fig. 7 shifts slightly, but the ordering of the curves are the same and the general trends presented in Fig. 7 is the same. Thus the conclusion is not sensitive to the exact size of a "small grain".

The evolution of skewness with relative density, shown in Fig. 9, can also be explained in terms of the consumption of the smaller particles. For the broad normal PSDs the skewness increases rapidly initially as the smaller particles are consumed, causing the PSD to become asymmetric towards larger grain sizes. For the broad log-normal distributions the distributions is already skewed and it remains fairly constant. The skewness of the narrow PSDs is seen to decrease initially, which is caused by the increasing number of small particles, as shown in Fig. 7. After the small particles are then consumed by the large particles (i.e. for $\rho \geq 0.85$), the skewness increases sharply.

The picture that emerges from these microstructural evolution data is that grain growth in the samples with broad PSDs in the early stages of sintering eliminates the small grains quickly. This reduces both the total number and area of the necks between particles. This in turn reduces the region where vacancies are annihilated, leading to a decrease in densification rate. As the neck area is lost in the broad PSDs, grain growth by surface diffusion becomes the dominant microstructural evolution mechanism, leading to poor densification. For the samples with a narrow PSD, the smaller grains persist to higher densities preserving the particles necks for densification to continue. Not only does this result in higher final relative density, but also a more uniform microstructure.

3.4 Grain coordination number

The increase in coordination number with particle radius has been used to explain the decrease in densification rate for broad PSDs (8). In order to investigate this and compare with the small grain explanation presented above, the evolution in grain coordination number as a function of relative density for the different PSDs was determined. This is also of interest as Young's modulus, mechanical hardness and fracture toughness are directly proportional to the mean grain coordination number of a sample in the initial stage of sintering (19). The mean grain coordination number is plotted as a function of relative density for both types of distributions in Fig. 10.

While the mean coordination numbers of the different PSDs initially range from 7 to 8 at relative density of ρ =0.67, they all become very similar at densities above ρ =0.80. Initially the broad distributions have the lowest mean coordi-

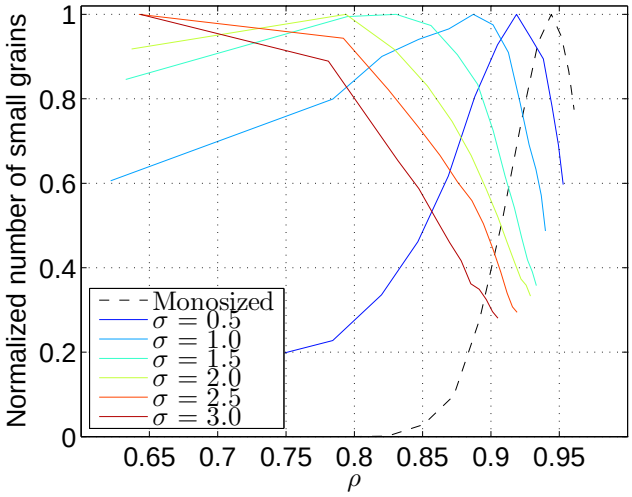

(a) Normal distributions

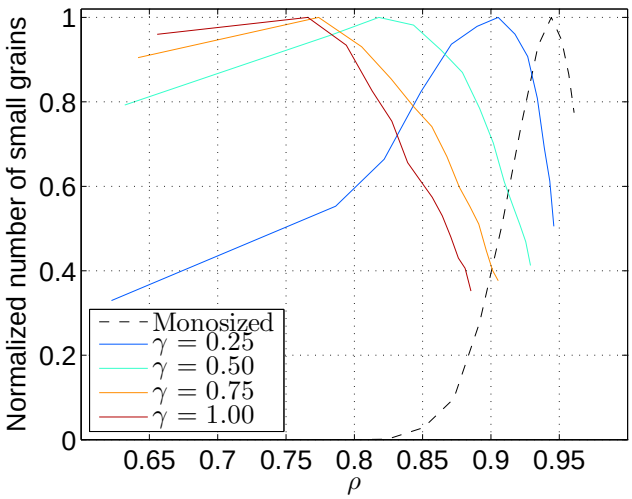

(b) Log-normal distributions

Figure 7. The number of small grains, i.e. grains with $G < 0.9\overline{G}$, for (a) the normal and (b) log-normal distributions as a function of relative density.

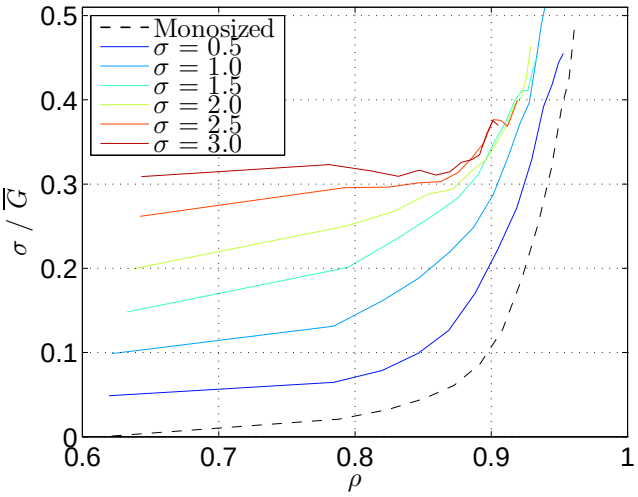

(a) Normal distributions

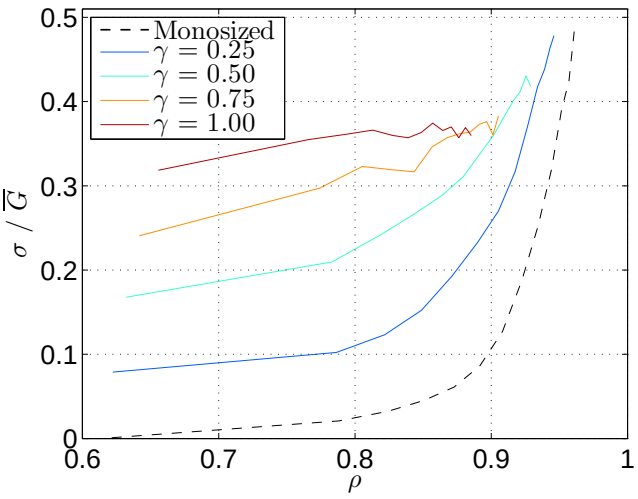

(b) Log-normal distributions

Figure 8. The standard deviation normalized by the average particle size as a function of relative density for (a) the normal and (b) log-normal distributions.

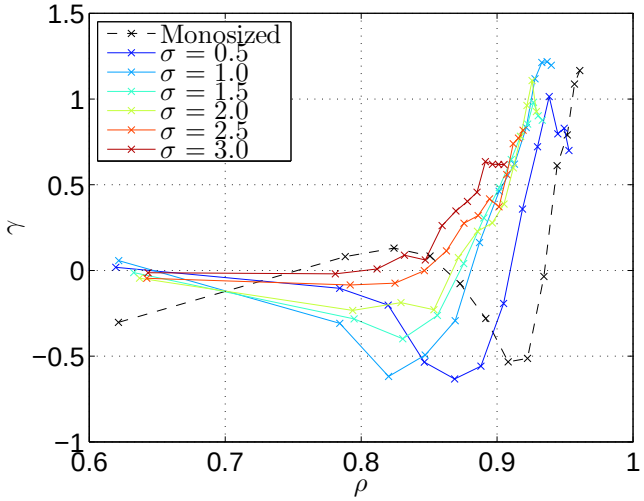

(a) Normal distributions

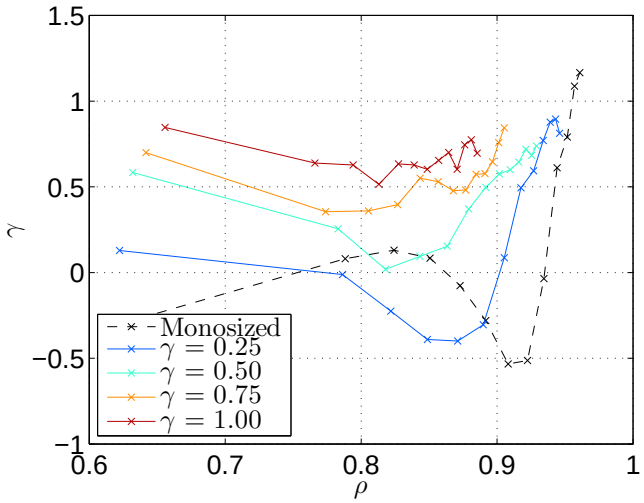

(b) Log-normal distributions

Figure 9. The skewness, γ, as a function of relative density for (a) the normal and (b) log-normal distributions.

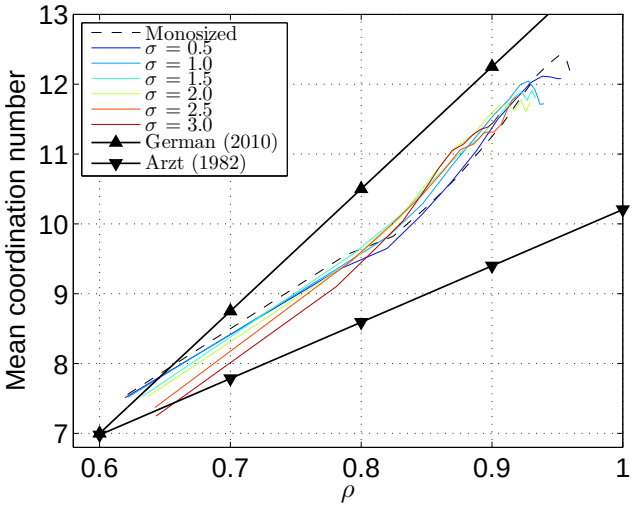

(a) Normal distributions

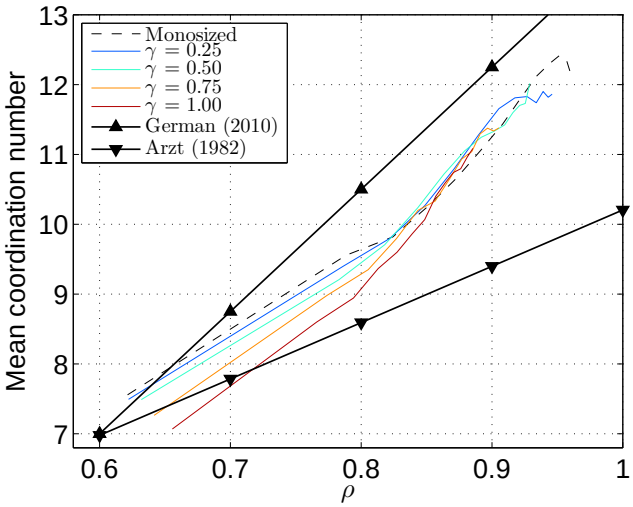

(b) Log-normal distributions

Figure 10. The mean grain coordination number as a function of the relative density for (a) the normal and (b) log-normal distributions.

nation number, but as sintering progresses the coordination number increases faster for these distributions. The reason the broader distributions have low initial mean coordination number is that large particles occupy the space where several smaller grains could have been placed which, in effect, would increase the coordination number of the system. The opposite, i.e. that the coordination number increases as the number of large particles increases, is argued by Yeh & Sacks (2) and Wonisch et. al. (8). They argue that large particles have high coordination number, which is true, but this does not mean the average coordination number increases for the distribution. Here it can be seen that coordination number actually decreases for broad distributions, in agreement with Suzuki & Oshima (20) and Yang et. al. (21).

A relation for the coordination number as a function of relative density has been proposed by both Arzt (22) and German (23) for monosized spherical particles. Both are linear expressions of the form $C_n = a * \rho + b$, where C_n is the mean coordination number, ρ is the relative density, and a and b are coefficients. The coefficients in Arzt (22) are $a = 8.07$ and $b = 2.14$, while in German (23) they are $a = 17.8$ and $b = -3.8$. Both of these relationships are shown in Fig. 10. Interestingly, they under- and over-estimates the evolution of the mean coordination number found here. The best fit for the parameters for the monosized distribution are $a = 15.0 \pm 1.9$ and $b = -2.2 \pm -1.7$.

German (24) argues that the high grain growth rate with increased relative density can be explained by an increased number of grain-grain contacts where coarsening can occur. This may explain the early grain growth in broad distributions, as the large grains have high coordination numbers, and thus can easily grow. However, care must be taken using this analysis. As illustrated by Fig. 10, the mean coordination number is lowest for the samples containing grains with the largest coordination numbers. One must consider the coordination number distribution in order to determine if a powder compact is likely to experience grain growth at low values of relative density.

While much attention has been given to grain coordination number and its effect on densification, our results do not bear this out. The grain coordination number of the initial powder compact showed some dependence on PSDs. However, as sintering progressed the mean coordination number were very similar in spite of the large difference in microstructure, grain size and pore configuration.

3.5 Sintering of PSD with lower grain boundary diffusivity

A duplicate set of simulations was conducted with the same initial microstructures but with a lower grain boundary diffusivity relative to surface diffusivity. It is well known that sintering in systems with high surface diffusivity to grain boundary diffusivity ratios results in coarsening of the particles with less densification (25; 26). However, we are not aware of any work that study sintering as a function of PSD in systems with high surface to grain boundary diffusivity ratio. The overall trend in grain growth and densification was similar to those already presented, although grain growth started at lower relative densities, and both densification rates and relative densities are much lower. This is consistent with previous work showing grain growth with less densification for higher surface diffusivity (25; 26). The detailed characterization of PSDs and their evolution during sintering are not presented for brevity.

4. Discussion

In general agreement with previously reported results, the simulations in this study showed that increasing the width of the PSD lowered the final relative density. However, the experimental observations reported in literature are not entirely consistent. We observed the densification rate to increasing with decreasing distribution width. This result is in agreement with Chappell et al. (10) but in disagreement with Yeh & Sacks (9) and Wonisch et al (8). The latter authors reported initially higher densification rate for the broad PSDs. Patterson and Griffin (1) reported the highest initial densification rates for the narrowest and broadst PSDs. However, all previous investigators reported much lower densification rates for broad PSDs during the later stages of sintering, in agreement with the simulation results presented here. The discrepancies in the initial densification rates may be due differences the initial powder size and shape characteristics. The simulations in this work have the advantage of having no agglomerations or packing defects, which are difficult to duplicate in experiments.

Unlike the findings of Wonisch et al. (8), the decrease in densification rate is greatest for the log-normal distribution and not the normal distribution. We attribute this difference to the fact that the mode was kept constant in this work, whereas Wonisch et al. kept the mean constant while skewness was increased. Another reason for the discrepancy may be that the DEM model is not able to capture true microstructural evolution as densification behavior is not based on the local curvatures and as the spherical particles are overlapped to simulate densification. The kMC model is able to replicate a microstructure and its evolution during sintering and thus to provide much more detailed information.

The narrow PSDs had the most uniform and homogeneous microstructures at the end of sintering. This is in agreement with the results of Patterson and Griffin (1). In many engineering applications this is desirable as the largest features often limit the engineering performance of the component.

In order to directly compare the sintering behavior of the normal and log-normal distributions, a power law of the form $\overline{G_{\text{norm}}} = a\rho^b + 1$, where a and b are parameters, was fitted to the average normalized grain size, $\overline{G_{\text{norm}}} = \overline{G}/\overline{G_0}$, as a function of relative density, ρ, for the different distributions, i.e. the curves shown in Fig. 5 normalized. The parameters a and b were determined using the least squares fitting method

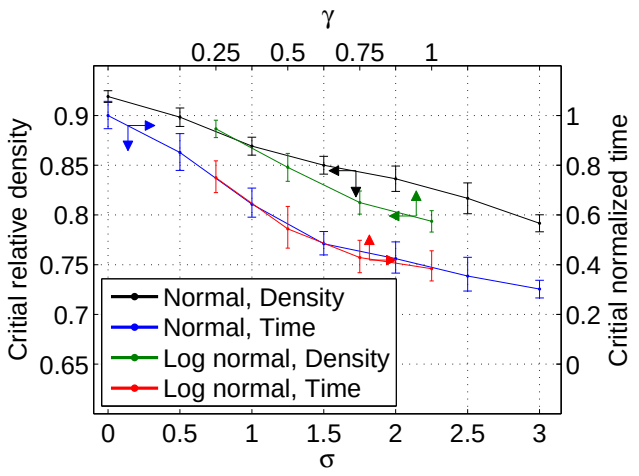

Figure 11. The critical relative density and normalized sintering time as function of the standard deviation, σ, or the skewness, γ. The distribution with $\sigma = 0$ is the monosized distribution. The small arrows on the graphs indicate which axis they correspond with. The error bars are a result of the power law fit used to determine the critical relative density.

with the R^2-parameter defined as

$$R^2 \equiv 1 - \frac{\sum_i (y_i - f_i)^2}{\sum_i (y_i - \bar{y})^2}, \qquad (1)$$

where y_i are the values of the data set, f_i are the interpolated values and $\bar{y}$ is the mean of the data. For the power law fits the R^2-value for all fits had a value above 0.99, indicating that the power law fits the data closely. The power law fits are used to determine the relative density at which $d\overline{G_{\text{norm}}}/d\rho = 1$, which is taken to be the relative density at which grain growth starts, termed the critical relative density at the corresponding time during sintering, termed critical time. Both of these are shown in Fig. 11 as a function of σ or γ. The critical relative density and critical time decrease as σ or γ increases. Comparing the normal and log-normal distributions it is seen that the critical relative density decreases faster compared to the critical time for the log-normal PSDs. The data presented in Fig. 11 support the view presented earlier. Grain growth begins earlier in the sintering cycle at lower densities for broad PSDs, reducing the number and area of grain necks available for densification by annihilation.

The results of the simulations presented suggest that PSDs can be used effectively to control the microstructure of the final sintered component. If a high relative density component with homogeneous microstructure is desired, then a narrow PSD powder will yield the best results. If lower relative density, but still uniform microstructure is desired, a narrow PSD powder sintered for less time to lower relative density is the best choice. If variations in microstructure with low relative density is desired, the exact microstructure can be tailored with a choice of PSDs.

5. Conclusion

A numerical kinetic Monte Carlo model has been used to study the sintering behavior of powder compacts of single grain spherical particles with different particle size distributions (PSDs). Powders compacts were generated numerically by randomly packing spherical particles of different PSDs. These PSDs were a single monosized, six normal and four log-normal distributions. For the normal distributions the mean value was fixed and the standard deviation, σ, was varied. For the log-normal distributions the mode was fixed and the skewness, γ, was varied. The sintering behavior, i.e. the densification rate and final relative density obtained, was found to be inversely proportional to σ and γ of the PSDs. The monosized particle compact had the fastest densification rate with the highest final relative density, while the broader distribution had progressively lower densification rates and final relative density with increasing σ and γ.

A detailed examination of the microstructural evolution revealed that the smallest grains in the broader distributions were consumed very quickly by larger neighboring grains. This behavior was also reflected in the relative standard deviation and skewness evolution of the PSDs. Eliminating the small grains reduces both the number and area of the necks between particles, which in turn reduces the region where vacancies are annihilated leading to a decrease in densification and densification rate. As the neck area is lost in the broad PSDs, grain growth by surface diffusion becomes the dominant microstructural evolution mechanism and leads to poor densification, while the narrow PSDs sinters to a higher relative density and also obtains a more uniform microstructure. It was also shown that broad PSDs have a larger pore intercept size, which can also contribute significantly to the early grain growth and poor densification observed for these distributions. Choosing and controlling the powder PSDs can thus be an effective way to control and tailor the microstructural evolution of a sintered component.

Acknowledgements

The authors would like to thank the Danish Council for Independent Research Technology and Production Sciences (FTP) which is part of The Danish Agency for Science, Technology and Innovation (FI) (Project # 09-072888) for sponsoring the OPTIMAC research work. Sandia National Laboratories is a multi-program laboratory managed and operated by Sandia Corporation, a wholly owned subsidiary of Lockheed Martin Corporation, for the U.S. Department of Energy's National Nuclear Security Administration under contract DE-AC04-94AL85000.

References

[1] B. R. Patterson and J. A. Griffin, "Effect of particle size distribution on sintering of tungsten," *Mod. Dev. Powder. Metall.*, **15** [4] 279-88 (1985).

[2] T. S. Yeh and M. D. Sacks, "Effect of particle size distribution on the sintering of alumina," *J. Am. Ceram. Soc.*, **71** [12] 484-7 (1988).

[3] F. S. Shiau, T. T. Fang and T. H. Leu, "Effect of particle-size distribution on the microstructural evolution in the intermediate stage of sintering," *J. Am. Ceram. Soc.*, **80** [2] 286-90 (1997).

[4] J. M. Ting and R. Y. Lin, "Effect of particle size distribution on sintering. Part I. Modelling," *J. Mat. Sci.*, **29** [7] 1867-72 (1994).

[5] J. M. Ting and R. Y. Lin, "Effect of particle size distribution on sintering. Part II. Sintering of alumina," *J. Mat. Sci.*, **30** [9] 2382-89 (1995).

[6] B.R. Patterson and L. A. Benson, "Effect of powder size distribution on sintering," *Prog. in Powder. Metall.*, **39** 215-30 (1984).

[7] J. Ma and L. C. Lim, "Effect of particle size distribution on sintering of agglomerate-free submicron alumina powder compacts," *J. Euro. Ceram. Soc.*, **22** [13] 2197-08 (2002).

[8] A. Wonisch, T. Kraft, M. Moseler and H. Riedel, "Effect of Different Particle Size Distributions on Solid-State Sintering: A Microscopic Simulation Approach," *J. Am. Ceram. Soc.*, **92** [7] 1428-34 (2009).

[9] M. F. Yan, R. M. Cannon, H. K. Bowen and U. Chowdhry, "Effect of Grain Size Distribution on Sintered Density," *Mat. Sci. Eng.*, **60** [3] 275-81 (1983).

[10] J. S. Chappell, T. A. Ring, J. D. Birchall, "Particle size distribution effects on sintering rates," *J. Appl. Phys.*, **60** [1] 383-91 (1986).

[11] V. Tikare, M. Braginsky, D. Bouvard and A. Vagnon, "Numerical simulation of microstructural evolution during sintering at the mesoscale in a 3D powder compact," *Comp. Mat. Sci.*, **48** [2] 317-25 (2010).

[12] F. Wakai and M. Yoshida and Y. Shinoda and T. Akatsu, "Coarsening and grain growth in sintering of two particles of different sizes," *Acta. Mater.*, **53** [5] 1361-71 (2005).

[13] C. G. Cardona, V. Tikare and S. J. Plimpton, "Parallel simulation of 3D sintering," *Int. J. Comp. Mat. Sci. Surf. Eng.*, **4** [1] 37-54 (2011).

[14] Y. Limoge and J. L. Bocquet, "Monte carlo simulation in diffusion studies: Time scale problems," *Acta. Metall.*, **36** [7] 1717-22 (1988).

[15] R. Bjørk, V. Tikare, H. L. Frandsen and N. Pryds, "The sintering behavior of close-packed spheres," *Scripta. Mater.*, **67** [1] 81-84 (2012).

[16] M. N. Rahaman, "Sintering of ceramics," CRC Press, 2008.

[17] R. J. McAfee Jr., "A Study Of Microstructural Evolution During Sintering Using Tessellation,", Ph.D. Thesis, University of Pittsburgh (2004)

[18] R. J. McAfee Jr. and I. Nettleship, "A mesoscale description of microstructural evolution for slip cast alumina sintered at 1350°C," *Ceram. Trans.*, **157** 105-114 (2005).

[19] Y. Boonyongmaneerat, "Mechanical properties of partially sintered materials," *Mat. Sci. Eng. A.*, **452** 773-80 (2007).

[20] M. Suzuki and T. Oshima, "Co-ordination number of a multi-component randomly packed bed of spheres with size distribution," *Powder. Tech.*, **44** [3] 213-18 (1985).

[21] A. Yang, C. T. Miller and L. D. Turcoliver, "Simulation of correlated and uncorrelated packing of random size spheres," *Phys. Rev. E.*, **54** [2] 1516-24 (1996).

[22] E. Arzt, "The influence of an increasing particle coordination on the densification of spherical powders," *Acta. Met.*, **30** [10] 1883-90 (1982).

[23] R. M. German, "Sintering Theory and Practice," Wiley-Interscience, 1996.

[24] R. M. German, "Coarsening in sintering: Grain shape distribution, grain size distribution, and grain growth kinetics in solid-pore systems," *Crit. Rev. Solid. State. Mate. Sci.*, **35** [4] 263-305 (2010).

[25] J. Svoboda and H. Riedel, "New solutions describing the formation of interparticle necks in solid-state sintering," *Acta. Metall. Mater.*, **43** [1] 1-10 (1995).

[26] F. Wakai and K. A. Brakke, "Mechanics of sintering for coupled grain boundary and surface diffusion," *Acta. Mater.*, **59** [14] 5379-87 (2011).